

Robust Stability and Performance Analysis of Incremental Dynamic-Inversion-Based Flight Control Laws

Pollack, Tijmen; van Kampen, Erik Jan

DOI

[10.2514/1.G006576](https://doi.org/10.2514/1.G006576)

Publication date

2023

Document Version

Final published version

Published in

Journal of Guidance, Control, and Dynamics

Citation (APA)

Pollack, T., & van Kampen, E. J. (2023). Robust Stability and Performance Analysis of Incremental Dynamic-Inversion-Based Flight Control Laws. *Journal of Guidance, Control, and Dynamics*, 46(9), 1785-1798. <https://doi.org/10.2514/1.G006576>

Important note

To cite this publication, please use the final published version (if applicable). Please check the document version above.

Copyright

Other than for strictly personal use, it is not permitted to download, forward or distribute the text or part of it, without the consent of the author(s) and/or copyright holder(s), unless the work is under an open content license such as Creative Commons.

Takedown policy

Please contact us and provide details if you believe this document breaches copyrights. We will remove access to the work immediately and investigate your claim.

Green Open Access added to TU Delft Institutional Repository

'You share, we take care!' - Taverne project

<https://www.openaccess.nl/en/you-share-we-take-care>

Otherwise as indicated in the copyright section: the publisher is the copyright holder of this work and the author uses the Dutch legislation to make this work public.



Robust Stability and Performance Analysis of Incremental Dynamic-Inversion-Based Flight Control Laws

Tijmen Pollack*[✉] and Erik-Jan van Kampen[†][✉]
Delft University of Technology, 2629 HS Delft, The Netherlands

<https://doi.org/10.2514/1.G006576>

Incremental nonlinear dynamic inversion (INDI) is a sensor-based control law design strategy that is based on the principles of feedback linearization. Contrary to its nonincremental counterpart (nonlinear dynamic inversion), this design method does not require a complete onboard model of the airframe dynamics and is therefore more robust against regular perturbations arising from aerodynamic variations. Therefore, INDI brings a natural design approach to desirable flying qualities. However, robustness against singular perturbations, which may arise due to transport delays, elastic airframe effects, or other types of badly modeled or unknown dynamics, is a known challenge for INDI-based control laws. Therefore, this paper addresses the question of robust stability and performance for INDI and its linear form (incremental dynamic inversion [IDI]) in the context of mixed regular and singular perturbations. This is done through analytical insights and by performing quantitative robustness assessments based on the structured singular value framework. Additionally, inversion loop augmentation solutions are investigated using robust synthesis techniques to improve the robustness characteristics of basic IDI designs.

I. Introduction

THE development of aircraft flight control laws is a comprehensive and multidisciplinary activity, one that is generally associated with significant effort and costs [1]. A primary reason is that flight control laws are subject to many, often conflicting design objectives and requirements associated with the intended mission and vehicle safety, which follow from overall program requirements and standards issued by airworthiness certification authorities [2,3]. This relates to several areas, including stability, flying qualities, structural mode interaction (SMI) [4], and structural loads, and need to be complied with across the range of possible aircraft flight envelopes and configurations, including failure conditions [2,3]. Consequently, the size and complexity of the development task is strongly dependent on the characteristics of the airframe and its desired capabilities.

In both the civil and military domains, industry has been able to successfully design and certify flight control laws for a wide range of vehicles and applications. Many of these designs are based on the *divide-and-conquer* philosophy, which relies on strictly linear design and analysis techniques applied to a range of linearized models of the airframe dynamics obtained over a grid of trim conditions throughout the flight envelope. Among these techniques are classical design methods such as one-loop-at-a-time frequency response shaping and root locus techniques, but also multivariable control law synthesis and analysis techniques that are able to capture the multivariable nature of the aircraft control problem, such as Linear-Quadratic-Regulation/Linear-Quadratic-Gaussian (LQR/LQG) and eigenstructure assignment design techniques [5–8]. However, the combination of more demanding operating capabilities and a general need for shorter and more efficient design cycles has put this proven design strategy under strain. The need for desirable flying qualities in (very) broad regions of the flight envelope results in extensive gain scheduling schemes that significantly increase the complexity of the result-

ing control law [9,10]. Moreover, design and tuning of these flight control laws is strongly tied to the dynamics of the bare airframe, which prohibits reuse over multiple airframes.

Nonlinear dynamic inversion (NDI) is a control law design technique that can address these challenges to a considerable extent. NDI-based control laws incorporate an onboard model (OBM) representation of the airframe dynamics, which allows the flying qualities design task to be performed in a largely isolated fashion. This natural advantage has been recognized by industry as well and represents a key feature that makes NDI attractive as a production control law design technique [10,11]. However, NDI-based control laws come with several challenges of their own, with robustness and (again) control law complexity being main areas of concern. For example, the aerodynamic database can grow very large in size, in particular when the aircraft can operate in many different flight conditions and configurations. At the same time, the control law needs to be robust against modeling and scheduling errors, which may take serious forms especially in those conditions where the airframe aerodynamics are nonlinear and known to only a limited extent.

Incremental nonlinear dynamic inversion (INDI) seeks to address these limitations by reducing the need for detailed and accurate onboard models of the airframe aerodynamics by using direct sensor measurements of the control variable derivatives instead. It is therefore also referred to as a sensor-based approach [12]. The only model information required by such control laws relates to the control effectiveness information for control allocation purposes. Since the early work on this simplified form of NDI [13,14], which only later became more commonly known as INDI [15], the ease of implementation of this technique and its ability to guarantee flying quality robustness in face of linear and nonlinear variations and uncertainties in the airframe aerodynamics have been demonstrated repeatedly both in-simulation (e.g., [16–24]) and during flight tests (e.g., [25–36]). In addition, analytical proofs of nominal and robust stability properties under external disturbances and regular perturbations have been established [12]. These achievements show that INDI has real benefits for use in future production aircraft.

However, research has also shown that INDI has relatively small stability robustness margins against singular perturbations [12] and ([37], Chap. 11) compared to traditional NDI. This includes time delays and other forms of known and unknown dynamics that increase the total system order and affect the sensor feedback paths [27,38,39]. In the context of the flight control development cycle, this implies that stability and SMI requirements may be difficult to meet in practice. Therefore, singular perturbations require special attention when examining the stability and performance robustness properties of INDI-based flight control laws. This is recognized by a growing volume of research [38,40–42]. For example, the authors of [40,41]

Presented as Paper 2022-1395 at the AIAA SciTech 2022 Forum, San Diego, CA, & Virtual, January 3–7, 2018; received 17 November 2021; revision received 25 July 2022; accepted for publication 3 June 2023; published online 28 July 2023. Copyright © 2023 by Delft University of Technology. Published by the American Institute of Aeronautics and Astronautics, Inc., with permission. All requests for copying and permission to reprint should be submitted to CCC at www.copyright.com; employ the eISSN 1533-3884 to initiate your request. See also AIAA Rights and Permissions www.aiaa.org/randp.

*Ph.D. Student, Control and Simulation Division, Faculty of Aerospace Engineering, Kluyverweg 1; t.s.c.pollack@tudelft.nl (Corresponding Author).

†Assistant Professor, Control and Simulation Division, Faculty of Aerospace Engineering, Kluyverweg 1; e.vankampen@tudelft.nl.

describe how the time delay margin of INDI-based control systems is affected in the presence of control effectiveness mismatch and actuator or filter dynamics, respectively.

Despite this growing interest in the INDI robustness question, many studies stay limited to the use of fixed-structure state-space model representations to perform robustness analysis. In other words, existing literature on this topic generally accepts that all model uncertainties and singular perturbation effects can be parameterized. However, it is well-known that this is fundamentally not the case for physical systems [43]. For example, the bare airframe dynamics of an aircraft are often difficult to model at high frequencies due to the presence of badly known or even unknown structural dynamics or unsteady aerodynamic effects [7,44,45]. Likewise, actuator systems generally show complex dynamics in the high-frequency range as well [7,44]. These are essentially nonparametric (or unstructured) effects, which can be modeled effectively by norm-bounded uncertainty descriptions [43]. To assess robust stability and performance levels adequately, such unstructured uncertainties need to be taken into account in the analysis model.

There are some studies on INDI that do consider the issue of robustness against unstructured uncertainties to a certain extent. One category relies on classical insights such as gain and phase margins (e.g., [27,46,47]). However, this yields little insight in case the system is affected by multiple uncertainties. This can be resolved by using norm-based arguments instead, as proposed in [42]. In this work it is assumed that the measurement error always remains bounded, which is a valid assumption to make in case the closed-loop control system remains stable. However, it does not provide any information about the conditions under which this assumption holds. Therefore, existing work in this direction does not give a complete picture about this aspect of INDI control design. This is in contrast to INDI-based controllers, for which more elaborate assessments have been reported based on, e.g., H_∞ -based analysis techniques [48–52].

Accordingly, the contributions of this work are as follows:

1) Stability and performance robustness properties of INDI-based flight control laws subject to regular and possibly unstructured singular perturbations are described in analytical form.

2) Robustness characteristics of basic linear incremental dynamic inversion (IDI) are quantified using the structured singular value (μ) framework.

3) Robust inversion loop design solutions that improve these properties are established using μ -synthesis.

The paper is structured as follows. Section II describes the basic robustness characteristics of INDI based on analytical insights from nonlinear and linear system formulations. This sets the stage for a numerical case study in Sec. III, where the robust stability and performance properties of IDI in its basic form are analyzed using the μ -framework in the context of a pitch rate control law for an open-access General Dynamics F-16 simulation model. This is followed by a discussion in Sec. IV, which is focused on augmentation techniques that enhance the robustness of basic IDI in a μ -optimal sense. The paper is concluded in Sec. V.

II. Fundamental Properties of Incremental Nonlinear Dynamic Inversion

In this section, the fundamental robustness characteristics of INDI are investigated and compared to its nonincremental counterpart based on analytical derivations and insights. First, the derivations of the control laws are reviewed in Sec. II.A. The subject of robustness to parametric and dynamic uncertainties in the nonlinear case is treated in Sec. II.B. Section II.C concentrates on the linear case to gain additional insights.

A. Control Law Design

INDI-based control laws follow the general principles of feedback linearization, which enables the construction of controllers in the sense of both input–output and full-state linearization for either regulation or tracking purposes for arbitrary relative degree [12,37]. Accordingly, consider a multi-input, multi-output, input-affine, nonlinear system Σ of the form

$$\Sigma: \begin{cases} \dot{\mathbf{x}} = \mathbf{f}(\mathbf{x}) + \mathbf{G}(\mathbf{x})\mathbf{u} \\ \mathbf{y} = \mathbf{h}(\mathbf{x}) \end{cases} \quad (1)$$

described by the state vector $\mathbf{x} \in \mathbb{R}^n$, the input vector $\mathbf{u} \in \mathbb{R}^m$, the observation vector $\mathbf{y} \in \mathbb{R}^m$, and smooth mappings \mathbf{f} , \mathbf{G} , and \mathbf{h} . Writing the system relative degree as $\boldsymbol{\rho} = [\rho_1, \dots, \rho_m]^T$, the output dynamics can be described as [12]

$$\begin{aligned} \mathbf{y}^{(\boldsymbol{\rho})} &= \begin{bmatrix} \mathcal{L}_f^{\rho_1} h_1(\mathbf{x}) \\ \vdots \\ \mathcal{L}_f^{\rho_m} h_m(\mathbf{x}) \end{bmatrix} \\ &+ \begin{bmatrix} \mathcal{L}_{g_1} \mathcal{L}_f^{\rho_1-1} h_1(\mathbf{x}) h_1(\mathbf{x}) & \dots & \mathcal{L}_{g_m} \mathcal{L}_f^{\rho_1-1} h_1(\mathbf{x}) \\ \vdots & \ddots & \vdots \\ \mathcal{L}_{g_1} \mathcal{L}_f^{\rho_m-1} h_m(\mathbf{x}) & \dots & \mathcal{L}_{g_m} \mathcal{L}_f^{\rho_m-1} h_m(\mathbf{x}) \end{bmatrix} \mathbf{u} \\ &= \boldsymbol{\alpha}(\mathbf{x}) + \mathbf{B}(\mathbf{x})\mathbf{u} \end{aligned} \quad (2)$$

where $\mathcal{L}_f^k h_i(\mathbf{x})$ and $\mathcal{L}_{g_i} \mathcal{L}_f^k h_i(\mathbf{x})$ represent repeated Lie derivatives of the function h_i along the vectors fields \mathbf{f} and \mathbf{g}_i , with \mathbf{g}_i being a column vector of the matrix \mathbf{G} [37]. For traditional feedback linearization, this expression can be used directly to construct a control law that linearizes the input–output dynamics to a set of $\sum_{i=1}^m \rho_i$ parallel integrators. Assuming that the control effectiveness matrix $\mathbf{B}(\mathbf{x})$ is invertible, the following control law is obtained:

$$\mathbf{u} = \hat{\mathbf{B}}^{-1}(\mathbf{x})[\boldsymbol{\nu} - \hat{\boldsymbol{\alpha}}(\mathbf{x})] \quad (3)$$

where $\hat{\boldsymbol{\alpha}}(\mathbf{x})$ and $\hat{\mathbf{B}}(\mathbf{x})$ represent onboard model estimates of $\boldsymbol{\alpha}(\mathbf{x})$ and $\mathbf{B}(\mathbf{x})$, respectively, and $\boldsymbol{\nu} \in \mathbb{R}^m$ is the pseudo-control vector generated by an auxiliary control law that is designed to meet the control objectives. To obtain an analogous control law in incremental form instead, one common approach is to perform a Taylor expansion of the output dynamics around the system state at time $t - \Delta t$ [12,53], where Δt represents the sampling interval. Denoting this condition by the subscript 0 for ease of notation yields the expression

$$\mathbf{y}^{(\boldsymbol{\rho})} = \mathbf{y}_0^{(\boldsymbol{\rho})} + \left. \frac{\partial[\boldsymbol{\alpha}(\mathbf{x}) + \mathbf{B}(\mathbf{x})\mathbf{u}]}{\partial \mathbf{x}} \right|_0 \underbrace{(\mathbf{x} - \mathbf{x}_0)}_{\Delta \mathbf{x}} + \mathbf{B}(\mathbf{x}_0) \underbrace{(\mathbf{u} - \mathbf{u}_0)}_{\Delta \mathbf{u}} + \mathbf{R}_1 \quad (4)$$

where \mathbf{R}_1 represents the expansion remainder. Consequently, the time-scale separation assumption can be leveraged to design the incremental control input $\Delta \mathbf{u}$, which assumes that all state-dependent and residual terms can be neglected [12,15,27,38]. This is typically justified in case high sampling rates and high-bandwidth actuators are available. The control law is completed by adding the control vector \mathbf{u}_0 to the resulting incremental term:

$$\mathbf{u} = \mathbf{u}_0 + \hat{\mathbf{B}}^{-1}(\mathbf{x}_0) \left[\boldsymbol{\nu} - \mathbf{y}_0^{(\boldsymbol{\rho})} \right] \quad (5)$$

Note that compared to its nonincremental counterpart from Eq. (3), the resulting control law does not require any model information on $\boldsymbol{\alpha}(\mathbf{x})$ but uses sensor feedback of the previous control vector and the derivative of the control variable instead. It has been demonstrated by other authors that the incremental form can also be leveraged for the more general class of nonlinear systems that are not affine in the input [53].

B. Robustness Properties

Let the true output dynamics associated with the system described by Eq. (1) be formulated as

$$\mathbf{y}^{(\boldsymbol{\rho})} = [\hat{\boldsymbol{\alpha}}(\mathbf{x}) + \boldsymbol{\xi}(\mathbf{x})] + [\hat{\mathbf{B}}(\mathbf{x}) + \boldsymbol{\Xi}(\mathbf{x})]\mathbf{u} \quad (6)$$

where the mappings ξ and Ξ represent additive regular perturbation terms that, by definition, do not change the order n of the system [12]. These terms represent known or unknown variations with respect to the model representations that are embedded in the dynamic inversion control law and are assumed to be bounded. The system input is modeled as the control law output perturbed by a possibly uncertain causal linear mapping Δ , which relates bounded input signals $z \in \mathbb{R}^m$ to bounded outputs $w = \Delta z \in \mathbb{R}^m$ [37]. This perturbation represents a class of unmodeled or neglected dynamics that exist in cascade with the system described by Eq. (1) and may be associated with actuation devices or neglected high-order structural modes (e.g., [7,9]). In the case of traditional NDI, the input then takes the form of

$$u = (I + \Delta)\hat{B}^{-1}(x)[\nu - \hat{\alpha}(x)] \quad (7)$$

Substituting this expression in Eq. (6) results in the following description of the closed-loop dynamics [9]:

$$y^{(\rho)} = \nu + (\xi(x) + \mathcal{D}(x, \Delta)[\nu - \hat{\alpha}(x)]) \triangleq \nu + \epsilon_{\text{NDI}}(x, \nu, \Delta) \quad (8)$$

where the term $\mathcal{D}(x, \Delta)$ is given by

$$\mathcal{D}(x, \Delta) = \Xi(x)\hat{B}^{-1}(x) + \hat{B}(x)\Delta\hat{B}^{-1}(x) + \Xi(x)\Delta\hat{B}^{-1}(x) \quad (9)$$

The residual term ϵ_{NDI} is in analogy with the terminology introduced in [12] and represents the closed-loop residual dynamics that emerge due to nonideal dynamic inversion in the presence of regular and dynamic perturbations. In consequence of the assumptions made earlier on the boundedness of the individual terms, ϵ_{NDI} has an upper bound $\bar{\epsilon}_{\text{NDI}}$ at a given state x under bounded virtual control ν . However, its magnitude can be relatively large, which indicates poor robustness properties. This is a widespread concern for control laws based on model-based NDI [10,12,37].

Considering the incremental form, a more general situation is considered to be able to analyze the effect of multiple dynamic perturbations in different locations of the feedback system. Writing $u_0 = (I + \Delta_1)u$ and $y_0^{(\rho)} = (I + \Delta_2)y^{(\rho)}$, with Δ_i representing causal, linear mappings as before and assuming that $x_0 = x$, the system input associated with the INDI-based control law given by Eq. (5) can be expressed as

$$u = (I + \Delta_1)u + \hat{B}^{-1}(x)[\nu - (I + \Delta_2)y^{(\rho)}] \quad (10)$$

It must be remarked that the standard relations $u_0 = z^{-1}u$ and $y_0^{(\rho)} = z^{-1}y^{(\rho)}$ are recovered in the special case when $\Delta_1 = \Delta_2 = (z^{-1} - 1)I$. An important advantage of this form is that it can be used to analyze the impact of perturbations that belong to the class of linear systems on the stability and robustness properties of INDI-based control systems. In particular, it enables direct analysis of the *synchronization effect*, which is notorious for incremental control laws and has been reported repeatedly in the literature [25,27,38]. This phenomenon typically has a profound impact on the closed-loop dynamics and originates from a discrepancy between the time of arrival of the output derivative and input feedback signals in the incremental inversion loop. The importance of this timing lies in the fact that the Taylor expansion in the control law derivation is performed around a single instant in time. Subsequently, by using Eq. (10) in combination with the relationship between u and \dot{y} from Eq. (6), an explicit description of the closed-loop output dynamics can be found:

$$y^{(\rho)} = \nu + \mathcal{S}(x, \Delta_1, \Delta_2)^{-1}[\mathcal{D}_1(x, \Delta_1)(\nu - [\hat{\alpha}(x) + \xi(x)]) - \Delta_2\nu] \triangleq \nu + \epsilon_{\text{INDI}}(x, \nu, \Delta_1, \Delta_2) \quad (11)$$

where $\mathcal{S}(x, \Delta_1, \Delta_2)$ and $\mathcal{D}_1(x, \Delta_1)$ are given by

$$\mathcal{S}(x, \Delta_1, \Delta_2) \triangleq I - \mathcal{D}_1(x, \Delta_1) + \Delta_2 \quad (12)$$

$$\mathcal{D}_1(x, \Delta_1) \triangleq \hat{B}(x)\Delta_1(\hat{B}(x) + \Xi(x))^{-1} \quad (13)$$

This result sheds light on several robustness properties. In particular, if u and $y^{(\rho)}$ can be measured accurately, the closed-loop system will be highly robust against regular perturbations in the output dynamics. If the \mathcal{L}_2 -gain of the perturbations Δ_i is expressed as γ_i , then it follows from Eqs. (11) and (13) that

$$\begin{aligned} \|\epsilon_{\text{INDI}}\|_2 &= \|\mathcal{S}(x, \Delta_1, \Delta_2)^{-1}[\mathcal{D}_1(x, \Delta_1)(\nu - [\hat{\alpha}(x) + \xi(x)]) - \Delta_2\nu]\|_2 \\ &\leq \gamma_{S_i} \cdot \left(\gamma_1 \|\hat{B}(x)(\hat{B}(x) + \Xi(x))^{-1}\|_2 \|\nu - [\hat{\alpha}(x) + \xi(x)]\|_2 \right. \\ &\quad \left. + \gamma_2 \|\nu\|_2 \right) \end{aligned} \quad (14)$$

where γ_{S_i} represents an upper bound on the \mathcal{L}_2 -gain of $\mathcal{S}(x, \Delta_1, \Delta_2)^{-1}$. One can deduce from this expression that the upper bound on $\|\epsilon_{\text{INDI}}\|$ goes towards zero[‡] as $\gamma_i \rightarrow 0$, independently of $\xi(x)$ and $\Xi(x)$. This shows that the nature of the robustness of INDI lies in the quality of sensor measurements and to a lesser extent on the onboard model. However, it is also found that the inverse mapping \mathcal{S}^{-1} needs to be bounded for ϵ_{INDI} to remain bounded at a given state x , which limits the permissible perturbation dynamics for which a stable control loop can be obtained. This is a direct manifestation of the synchronization effect and requires careful consideration by the designer. Considering the case where Δ_1 approaches zero, e.g., ϵ_{INDI} will grow unbounded if $\Delta_2 \rightarrow -I$. This is in contrast with traditional NDI, for which an upper bound on the inversion residual can always be found under the assumptions stated earlier. Therefore, boundedness of \mathcal{S}^{-1} represents an important aspect of the stability of an INDI-based control system. Accordingly, an appropriate design solution is to ensure that $\mathcal{D}_1(x, \Delta_1) = \Delta_2$, in which case it holds that $\mathcal{S} = I$ and

$$\epsilon_{\text{INDI}}(x, \Delta_2) = -\Delta_2[\hat{\alpha}(x) + \xi(x)] \quad (15)$$

This idea will be referred to as the *matching strategy* and is in line with the main design philosophy that has been adopted in the past [25,27,38]. It should be noted that this approach is feasible only when the control effectiveness and singular perturbation dynamics are completely known. With this procedure, the inversion residual will be nonzero for nonzero Δ_2 . Nevertheless, the norm of ϵ_{INDI} will be small if Δ_2 is small in magnitude in the operating time-scale of Σ , which is in line with the time-scale separation assumption that underlies the derivation of the control law.

C. Linear State Space Insights

The basic robust stability and performance properties of INDI can be further understood by analyzing the state space representation of the closed-loop dynamics in case the plant Σ and the control law are linear. For simplicity, it will be assumed in this subsection that the system features a common relative degree equal to one. Such a system is closely representative of the equations of motion of the rotational rates of an aircraft. Accordingly, the plant dynamics can be written in normal form [54] as follows:

$$\Sigma: \begin{cases} \dot{\zeta} &= R\zeta + T\eta + Bu \\ \dot{\eta} &= P\zeta + Q\eta \\ y &= \zeta \end{cases} \quad (16)$$

Writing the perturbed feedback signals as $u_0 = u + w_1$ and $\dot{\zeta}_0 = \dot{\zeta} + w_2$, it follows immediately from the control law formulation that

$$u = u_0 + \hat{B}^{-1}(\nu - \dot{\zeta}_0) = u + w_1 + \hat{B}^{-1}(\nu - \dot{\zeta} - w_2) \rightarrow \dot{\zeta} = \nu + \hat{B}w_1 - w_2 \quad (17)$$

[‡]It should be remarked that the control effectiveness matrix shall not become singular. Moreover, the presence of, e.g., actuator dynamics and finite sampling times generally implies that $\gamma_i \geq 1$ in practical situations.

where w_i are given as

$$\begin{aligned} w_1 &= \Delta_1 z_1 = \Delta_1 u = \Delta_1 B^{-1}(\dot{\zeta} - R\zeta - T\eta) \\ w_2 &= \Delta_2 z_2 = \Delta_2 \dot{\zeta} = \Delta_2(\nu + \hat{B}w_1 - w_2) \end{aligned} \quad (18)$$

Here, the last equalities follow directly from the output dynamics descriptions given by Eqs. (16) and (17). Using the above expressions for $\dot{\zeta}$, $\dot{\eta}$, z_1 , and z_2 and using the fact that $\epsilon_{\text{IDI}} \triangleq \dot{\zeta} - \nu$, the closed-loop dynamics of the inversion residual are described by

$$\begin{aligned} \begin{bmatrix} \dot{\zeta} \\ \dot{\eta} \\ \epsilon_{\text{IDI}} \\ z_1 \\ z_2 \end{bmatrix} &= \begin{bmatrix} \mathbf{0} & \mathbf{0} & I & \hat{B} & -I \\ P & Q & \mathbf{0} & \mathbf{0} & \mathbf{0} \\ \mathbf{0} & \mathbf{0} & \mathbf{0} & \hat{B} & -I \\ -B^{-1}R & -B^{-1}T & B^{-1} & B^{-1}\hat{B} & -B^{-1} \\ \mathbf{0} & \mathbf{0} & I & \hat{B} & -I \end{bmatrix} \begin{bmatrix} \zeta \\ \eta \\ \nu \\ w_1 \\ w_2 \end{bmatrix}, \\ \begin{bmatrix} w_1 \\ w_2 \end{bmatrix} &= \begin{bmatrix} \Delta_1 & \mathbf{0} \\ \mathbf{0} & \Delta_2 \end{bmatrix} \begin{bmatrix} z_1 \\ z_2 \end{bmatrix} \end{aligned} \quad (19)$$

This formulation enables direct verification of the stability of the closed-loop system and the performance properties of the mapping from ν to ϵ_{IDI} for all perturbations. Likewise, if Δ_i represents a series interconnection of two dynamic systems Γ_i and $\bar{\Delta}_i$, where it is known that $\|\bar{\Delta}_i\|_\infty \leq 1$ and

$$\Gamma_i: \begin{cases} \dot{q}_i = A_i q_i + B_i z_i \\ \bar{z}_i = C_i q_i + D_i z_i \end{cases} \quad (20)$$

then, Eq. (19) extends to

$$\begin{aligned} \begin{bmatrix} \dot{\zeta} \\ \dot{\eta} \\ \dot{q}_1 \\ \dot{q}_2 \\ \epsilon_{\text{IDI}} \\ \bar{z}_1 \\ \bar{z}_2 \end{bmatrix} &= \begin{bmatrix} \mathbf{0} & \mathbf{0} & \mathbf{0} & \mathbf{0} & I & \hat{B} & -I \\ P & Q & \mathbf{0} & \mathbf{0} & \mathbf{0} & \mathbf{0} & \mathbf{0} \\ -B_1 B^{-1}R & -B_1 B^{-1}T & A_1 & \mathbf{0} & B_1 B^{-1} & B_1 B^{-1}\hat{B} & -B_1 B^{-1} \\ \mathbf{0} & \mathbf{0} & \mathbf{0} & A_2 & B_2 & B_2 \hat{B} & -B_2 \\ \mathbf{0} & \mathbf{0} & \mathbf{0} & \mathbf{0} & \mathbf{0} & \hat{B} & -I \\ -D_1 B^{-1}R & -D_1 B^{-1}T & C_1 & \mathbf{0} & D_1 B^{-1} & D_1 B^{-1}\hat{B} & -D_1 B^{-1} \\ \mathbf{0} & \mathbf{0} & \mathbf{0} & C_2 & D_2 & D_2 \hat{B} & -D_2 \end{bmatrix} \begin{bmatrix} \zeta \\ \eta \\ q_1 \\ q_2 \\ \nu \\ w_1 \\ w_2 \end{bmatrix}, \\ \begin{bmatrix} w_1 \\ w_2 \end{bmatrix} &= \begin{bmatrix} \bar{\Delta}_1 & \mathbf{0} \\ \mathbf{0} & \bar{\Delta}_2 \end{bmatrix} \begin{bmatrix} \bar{z}_1 \\ \bar{z}_2 \end{bmatrix} \end{aligned} \quad (21)$$

In this context, Γ_i represents an uncertainty weight that places an upper bound on the \mathcal{L}_2 -gain (or H_∞ -norm) of Δ_i . This expression is an example of the interconnection framework that enables evaluation of the linear robustness properties of IDI-based control systems, which is key to the norm-based analyses presented in Secs. III and IV.

As a special case, consider the situation where Δ_i is described by a deterministic (unity) input-output mapping. This implies that the perturbation dynamics can be described by a known form. Then, the closed-loop dynamics can be expressed as

$$\begin{aligned} \begin{bmatrix} \dot{\zeta} \\ \dot{\eta} \\ \dot{q}_1 \\ \dot{q}_2 \\ \epsilon_{\text{IDI}} \end{bmatrix} &= \begin{bmatrix} -S^{-1}\tilde{D}_1 R & -S^{-1}\tilde{D}_1 T & S^{-1}\hat{B}C_1 & -S^{-1}C_2 & S^{-1} \\ P & Q & \mathbf{0} & \mathbf{0} & \mathbf{0} \\ -B_1(SB)^{-1}E_1 R & -B_1(SB)^{-1}E_1 T & A_1 + B_1\tilde{S}^{-1}C_1 & -B_1(SB)^{-1}C_2 & B_1(SB)^{-1} \\ -B_2 S^{-1}\tilde{D}_1 R & -B_2 S^{-1}\tilde{D}_1 T & B_2 S^{-1}\hat{B}C_1 & A_2 - B_2 S^{-1}C_2 & B_2 S^{-1} \\ -S^{-1}\tilde{D}_1 R & -S^{-1}\tilde{D}_1 T & S^{-1}\hat{B}C_1 & -S^{-1}C_2 & S^{-1} - I \end{bmatrix} \begin{bmatrix} \zeta \\ \eta \\ q_1 \\ q_2 \\ \nu \end{bmatrix} \end{aligned} \quad (22)$$

where

$$S \triangleq I - \tilde{D}_1 + D_2, \quad \tilde{S} \triangleq \hat{B}^{-1}SB, \quad \tilde{D}_1 \triangleq \hat{B}D_1 B^{-1}, \quad E_1 \triangleq \tilde{D}_1 + S \quad (23)$$

Regarding the synchronization effect, the dynamics associated with the inverse map \mathcal{S}^{-1} appear directly in the lower-right part of the obtained system formulation. Alternatively, an equivalent description of these dynamics can be arrived at by performing a different derivation using Eqs. (11) and (12) as starting point. If \mathcal{S} is considered as a mapping between ϵ_{IDI} and some signal d , then its dynamics can be described as follows for the selected realizations of Γ_i and Δ_i :

$$\begin{aligned} \mathcal{S}: \begin{cases} \dot{q}_1 = A_1 q_1 + B_1 B^{-1} \epsilon_{\text{IDI}} \\ \dot{q}_2 = A_2 q_2 + B_2 \epsilon_{\text{IDI}} \\ d = (I - \mathcal{D}_1 + \Delta_2) \epsilon_{\text{IDI}} \\ \quad = -\hat{B}C_1 q_1 + C_2 q_2 + (I - \tilde{D}_1 + D_2) \epsilon_{\text{IDI}} \end{cases} \\ \rightarrow \mathcal{S}: \begin{bmatrix} \dot{q} \\ d \end{bmatrix} = \begin{bmatrix} A_S & B_S \\ C_S & D_S \end{bmatrix} \begin{bmatrix} q \\ \epsilon_{\text{IDI}} \end{bmatrix} \end{aligned} \quad (24)$$

Consequently, the dynamics of the inverse map \mathcal{S}^{-1} are found as

$$\begin{aligned} \mathcal{S}^{-1}: \begin{bmatrix} \dot{q} \\ \epsilon_{\text{IDI}} \end{bmatrix} &= \begin{bmatrix} A_S - B_S D_S^{-1} C_S & B_S D_S^{-1} \\ -D_S^{-1} C_S & D_S^{-1} \end{bmatrix} \begin{bmatrix} q \\ d \end{bmatrix} \\ &\triangleq \begin{bmatrix} A_{S_i} & B_{S_i} \\ C_{S_i} & D_{S_i} \end{bmatrix} \begin{bmatrix} q \\ d \end{bmatrix} \end{aligned} \quad (25)$$

Substituting and expanding terms yields

$$\mathbf{S}^{-1} : \begin{bmatrix} \dot{q}_1 \\ \dot{q}_2 \\ \epsilon_{\text{IDI}} \end{bmatrix} = \begin{bmatrix} A_1 + B_1 \tilde{S}^{-1} C_1 & -B_1 (SB)^{-1} C_2 & B_1 (SB)^{-1} \\ B_2 S^{-1} \hat{B} C_1 & A_2 - B_2 S^{-1} C_2 & B_2 S^{-1} \\ S^{-1} \hat{B} C_1 & -S^{-1} C_2 & S^{-1} \end{bmatrix} \times \begin{bmatrix} q_1 \\ q_2 \\ d \end{bmatrix} \quad (26)$$

Consequently, by substituting $d = \mathcal{D}_1(\nu - R\zeta - T\eta) - \Delta_2\nu$ as per Eq. (11) and reordering terms, another realization of the closed-loop dynamics represented by Eq. (22) will be obtained. Consequently, boundedness of \mathbf{S}^{-1} can be verified directly by checking if A_{S_i} is Hurwitz. This will be further discussed by means of two special cases.

1. *Strictly Proper Dynamics in the Feedback Path*

Consider that Γ_2 arises because of strictly proper dynamics in the feedback path, which is often the case in practice. In order for $\dot{\zeta}_0 = (\mathbf{I} + \Gamma_2)\dot{\zeta}$ to represent a strictly proper transfer function, it must hold that $D_2 = -\mathbf{I}$ as per Eq. (20). A direct result is that $S = \mathbf{0}$ if D_1 is zero, which leads to the conclusion that ϵ_{IDI} will be infinitely large in the limit in the absence of any compensating perturbation dynamics Γ_1 . Likewise, consider the case where both Γ_1 and Γ_2 arise due to proper dynamics in the feedback path, leading to $D_1 = D_2 = -\mathbf{I}$. Then, Eq. (22) reduces to

$$\begin{bmatrix} \dot{\zeta} \\ \dot{\eta} \\ \dot{q}_1 \\ \dot{q}_2 \\ \epsilon_{\text{IDI}} \end{bmatrix} = \begin{bmatrix} R & T & BC_1 & -K_B C_2 & K_B \\ P & Q & \mathbf{0} & \mathbf{0} & \mathbf{0} \\ \mathbf{0} & \mathbf{0} & A_1 + B_1 C_1 & -B_1 B^{-1} K_B C_2 & B_1 B^{-1} K_B \\ B_2 R & B_2 T & B_2 B C_1 & A_2 - B_2 K_B C_2 & -B_2 K_B \\ R & T & BC_1 & K_B C_2 & K_B - I \end{bmatrix} \times \begin{bmatrix} \zeta \\ \eta \\ q_1 \\ q_2 \\ \nu \end{bmatrix} \quad (27)$$

where $K_B \triangleq B\hat{B}^{-1}$. This result enables direct verification of the stability and performance properties of ϵ_{IDI} when subjected to parametric uncertainties in Γ_1 , Γ_2 , and the control effectiveness. If the eigenmodes associated with \mathbf{S}^{-1} are sufficiently distant from the eigenmodes of Σ , which can be argued to hold if the time-scale separation assumption holds, stability of the synchronization dynamics can be assessed by verifying if A_{S_i} is Hurwitz:

$$A_{S_i} = \begin{bmatrix} A_1 + B_1 C_1 & -B_1 B^{-1} K_B C_2 \\ B_2 B C_1 & A_2 - B_2 K_B C_2 \end{bmatrix} \quad (28)$$

Furthermore, if Σ and the control law do not feature any coupling between input–output channels, which holds for diagonal control systems, using the change of variables

$$q = \begin{bmatrix} \mathbf{I} & \mathbf{0} \\ \mathbf{0} & BI \end{bmatrix} \bar{q} \triangleq \Lambda \bar{q} \quad (29)$$

for each isolated control channel enables direct assessment of the synchronization dynamics without any information of Σ . In this case, the eigenvalues of A_{S_i} can be found for each channel based on

$$\bar{A}_{S_i} \triangleq \Lambda^{-1} A_{S_i} \Lambda = \begin{bmatrix} A_1 + B_1 C_1 & -k_B B_1 C_2 \\ B_2 C_1 & A_2 - k_B B_2 C_2 \end{bmatrix} \quad (30)$$

where the scalar nature of each channel is reflected by the scalar scaling factor k_B . This simple result can be used to directly assess the impact of proper high-order dynamics on ϵ_{IDI} . Since the scaling factor cannot be factored out from the expression, the synchronization dynamics will be affected if the control effectiveness undergoes unmodeled variations. This is independent from how Γ_1 and Γ_2 are selected.

2. *Digital Sampling and Time Delays*

The impact of the digital nature of the control system can also be assessed. It is assumed that high-order perturbing dynamics are absent. In this case, it holds that $\Gamma_i = z^{-1} - 1 = e^{-sT_s} - 1$. If the unit time delay is modeled as a first-order Padé approximation, then it holds that $e^{-sT_s} \approx (T_s/2s - 1/T_s/2s + 1)$. As a result, one realization of the state-space formulation of Γ_i is given as $A_i = -2/T_s$, $B_i = 2$, $C_i = 2/T_s$, and $D_i = -2$. Substituting terms then leaves the following description of A_{S_i} :

$$\bar{A}_{S_i} = \frac{1}{T_s(1 - k_B/2)} \begin{bmatrix} k_B & -2k_B \\ 2 & -(k_B + 2) \end{bmatrix} \quad (31)$$

which has eigenvalues with negative real part if and only if $0 < k_B < 2$. Therefore, stability cannot be achieved in this scenario if the modeled control effectiveness is either of opposite sign or too small compared to the true value. It should be noted that this is in agreement with the findings by [55] that ϵ_{INDI} remains bounded independently of $\zeta(x)$ if $\|\mathbf{I} - K_B\|_2 < 1$ in case only the digital nature of the control system is considered. However, these limits do not apply in the case of general perturbing dynamics, as reflected by Eq. (26). Moreover, the size of the sampling time affects overall closed-loop stability of the INDI control system as well. These findings are confirmed by the work reported in [40].

III. **Basic Incremental Dynamic Inversion Robustness Assessment**

This section focuses on H_∞ -based robustness assessments to perform quantitative comparisons of the robust stability and performance characteristics of linear INDI (IDI)-based flight control laws. The kind of interconnection machinery described in Sec. II.C is used to describe the generalized control system. Given the structured and mixed nature of the uncertainty formulation, the structured singular value (μ) is used in mixed form using DG -scales [43]. The MATLAB Robust Control Toolbox™ (version 6.9) is used as the primary software tool to this end [56]. The findings from this section are used to establish a benchmark to which the augmentation solutions discussed in Sec. IV can be compared. The design case study is described in Sec. III.A, which gives an overview of the control system elements and the design requirements. The robustness outcomes of standard dynamic inversion are discussed first in Sec. III.B, which is followed by an analogous evaluation of a basic IDI design in Sec. III.C.

A. **Problem Formulation**

The numerical evaluation is based on a linear dynamic-inversion-based pitch rate control law design for an open-access simulation model (low-fidelity version) of the General Dynamics F-16 [45,57] and is closely in line with the analysis presented in [7]. The nonlinear aircraft model has been trimmed and linearized around a flight condition of Mach 0.5 at 10,000 feet altitude, with the center of gravity located at 38% relative to the mean aerodynamic chord (MAC), resulting in a trim angle of attack of 2.6 deg. Therefore, the scope is limited to a single flight condition that is well within the interior of the service flight envelope. To simplify the analysis, the linear model is reduced to the short-period mode only. It is assumed

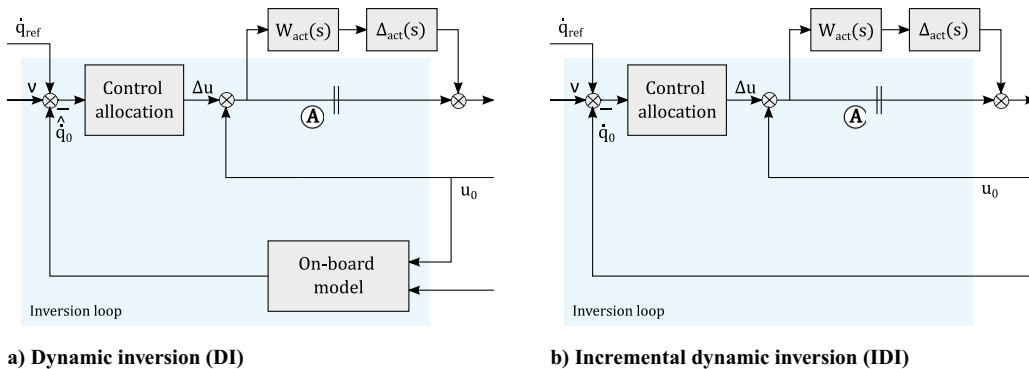


Fig. 2 Basic inversion architecture block diagrams.

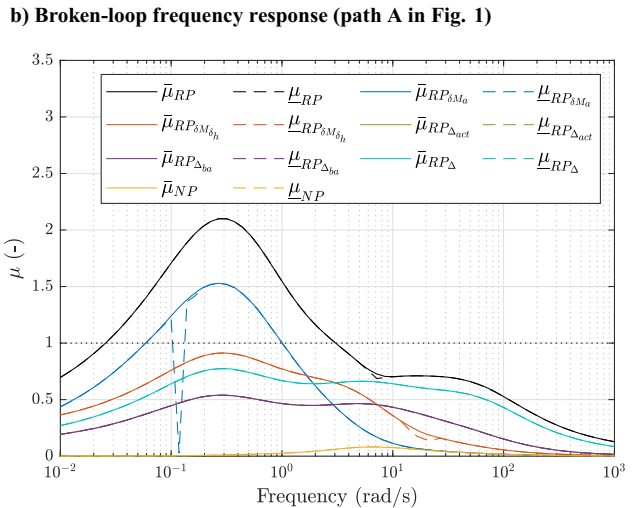
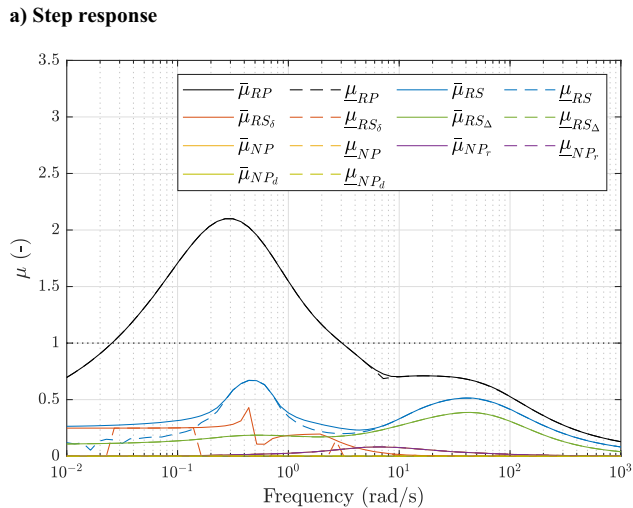
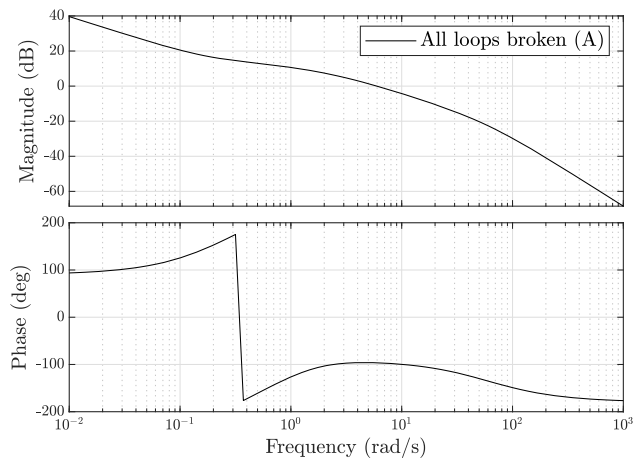
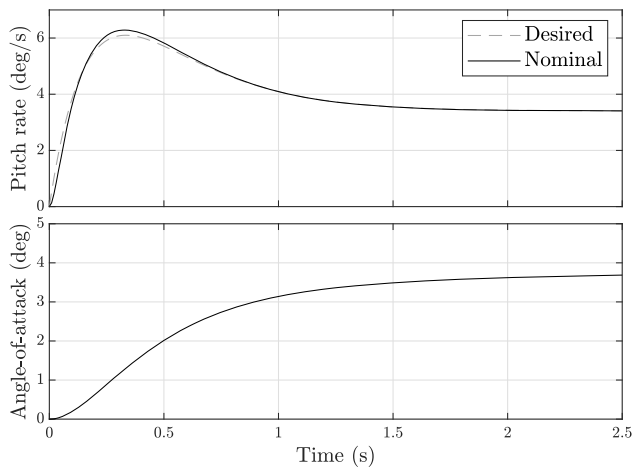


Fig. 3 Overview of basic DI-based control system properties.

uncertainty set, the performance requirements are not. In the low-to-medium frequency region, the robust performance deficit is dominated by parametric uncertainty in the stability and control derivatives; by contrast, robust stability and performance levels at medium-to-high frequencies are constrained by the dynamic actuator and airframe uncertainties. It must be noted that increasing the outer loop gain improves robustness to aerodynamic uncertainty at the cost of robust stability at high frequencies.

C. Incremental Dynamic Inversion

The same analysis is performed to examine the robustness properties of a basic variant of the incremental dynamic inversion architecture. This implementation does not include any additional processing

of the horizontal tail position and angular acceleration measurements, which implies that the synchronization compensation and acceleration estimation blocks in Fig. 1 are unity in this case. Figures 4a and 4b show the step response and broken-loop frequency responses (path locations indicated in Fig. 1) of the basic IDI-based control law. These are equivalent to the model-based dynamic inversion control system, except for the broken-loop response after closing the actuator feedback loop(s). The latter reveals that applying IDI effectively results in a high-gain control system at the level of the bare airframe, which explains its robustness to aerodynamic uncertainties. This observation is confirmed by the μ -analysis, as shown in Figs. 4c and 4d. Attainable robust performance levels are significantly improved in the low-to-medium frequency range compared to

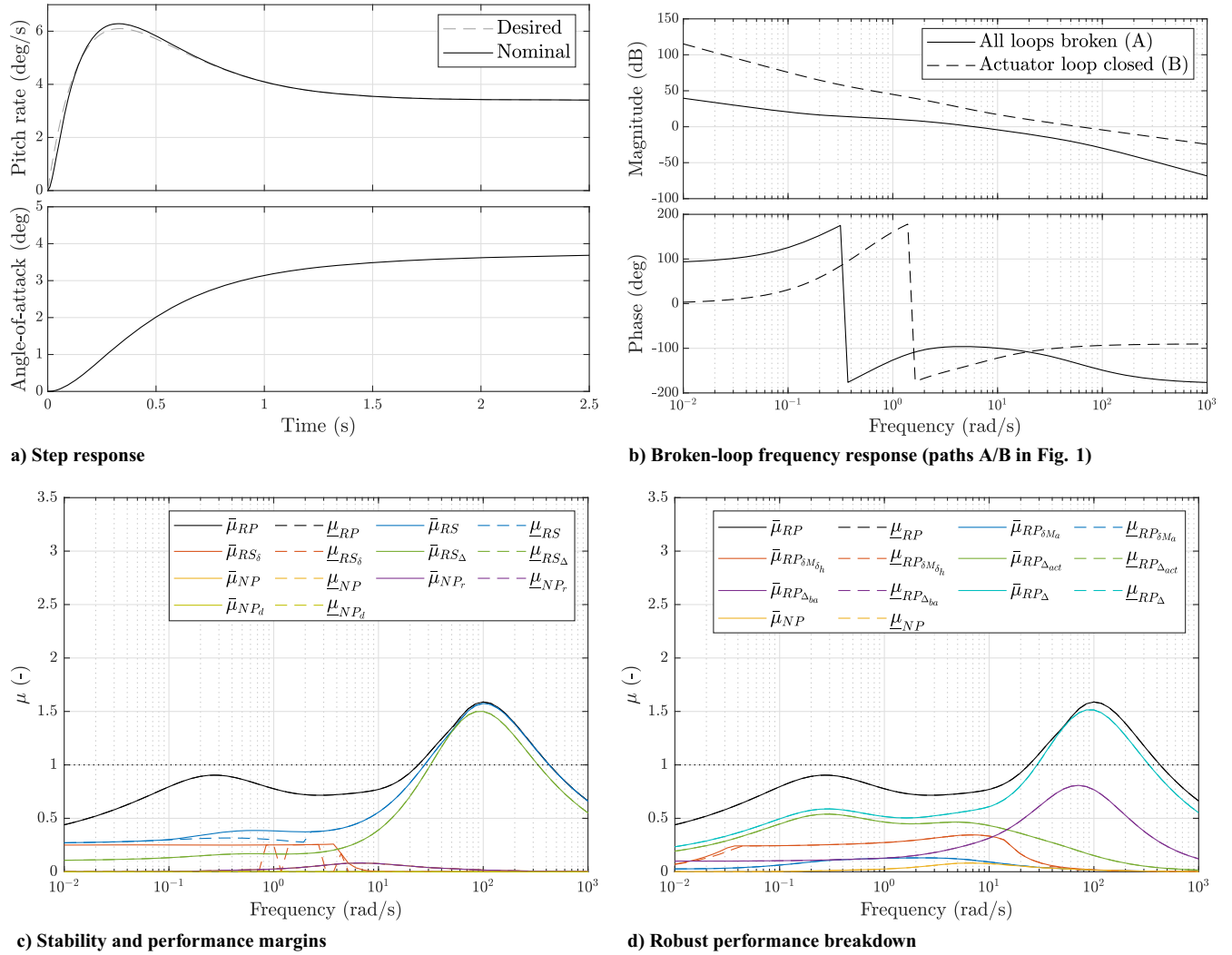


Fig. 4 Overview of basic IDI-based control system properties.

dynamic inversion, which can be directly attributed to the increased robustness to aerodynamic variations. However, this comes at the cost of robust stability, which cannot be met as a result of the dynamic actuator and airframe uncertainties and represents a direct manifestation of the synchronization effect described in Secs. II.B and II.C. Note that this result also confirms that outer loop regulator gains can be reduced when INDI is adopted. This is in line with the notion that incremental control action mitigates steady-state error and has been reported earlier in the literature [27].

IV. Robust Incremental Dynamic Inversion Augmentation Techniques

In this section, inversion loop augmentation techniques that improve the basic robustness properties of IDI-based control system designs are investigated within the context of the F-16 short-period design problem. Consistent with the basic inversion architectures discussed previously, direct pitch acceleration measurements are again used in the control design. However, thanks to the presented problem formulation, the outcomes are also applicable to solutions that adopt differentiated pitch rate instead. Three principal design degrees of freedom form the basis of the discussion. The angular acceleration and synchronization filter design elements are considered first in Sec. IV.A, where full-order (unstructured) mixed μ -synthesis based on *DGK*-iteration [43] is used to leverage full design flexibility. The MATLAB Robust Control Toolbox™ [56] is again used to this end. This is followed by an investigation of structured filter designs in Sec. IV.B, where the scope is limited to

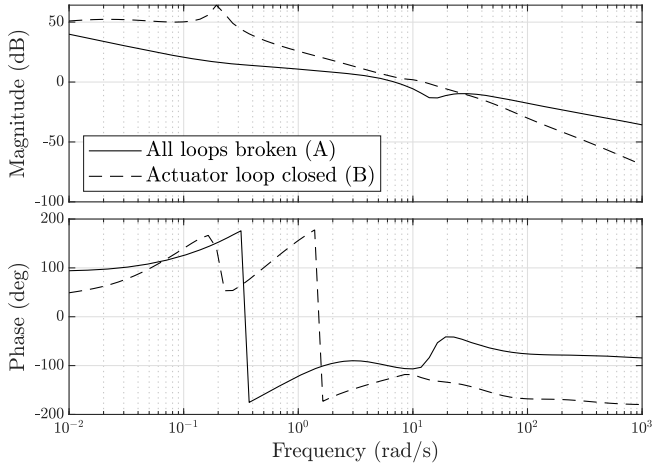
configurations that exploit the matching strategy. Section IV.C focuses on hybrid implementations, where supplemental model information is used as an additional form of augmentation of the basic incremental inversion loop. Section IV.D concludes the discussion.

A. The μ -Optimal Full-Order Inversion Feedback Filter Design

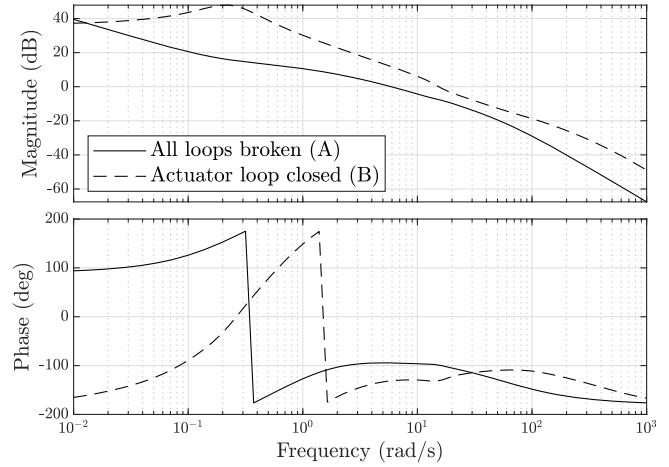
The preceding sections have highlighted that adequate compensation of the synchronization effect forms a key factor in the design of incremental control laws. Section II.B explained the relevance of the mapping \mathcal{S} and introduced the matching procedure as a simple, but effective method to improve stability. In case of uncertainty, accurately matching perturbing dynamics is not possible. Therefore, it is of interest to assess how the synchronization effect shall be accounted for in a μ -optimal fashion in light of the regular and dynamic uncertainties and performance requirements that define the control system design problem. This comes down to the question how this translates to the design of the acceleration estimation and synchronization estimation filters as shown in the general inversion architecture of Fig. 1. The following asynchronous and synchronous filter design architectures are considered in this respect:

$$v_f^{(\text{async})} = K(\dot{q}_0, \delta_{h,0}), \quad v_f^{(\text{sync})} = K(v_0) \quad (38)$$

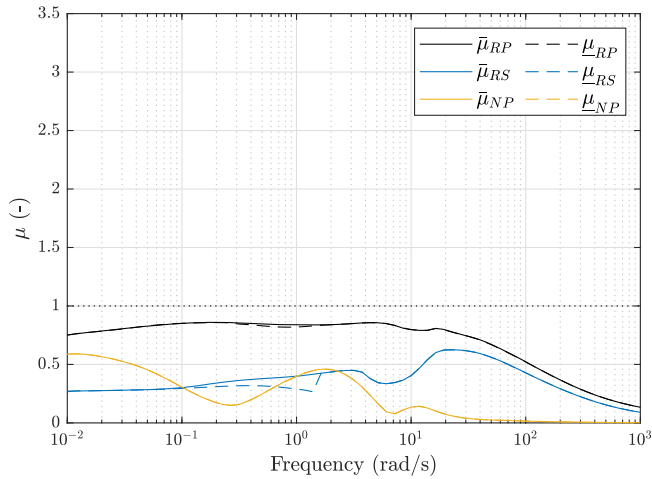
where K represents the feedback filter augmentation system and v forms the combined IDI feedback signal including control allocation. Accordingly, the input to the synchronous filter is given by



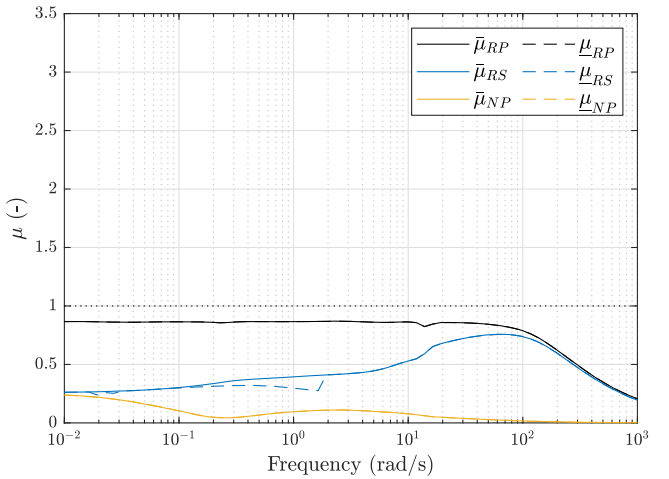
a) Broken-loop frequency response (asynchronous)



b) Broken-loop frequency response (synchronous)



c) Stability and performance margins (asynchronous)



d) Stability and performance margins (synchronous)

Fig. 5 Full-order μ -optimal augmented IDI-based control system properties.

$$v_0 = \frac{1}{\hat{m}_{\delta_h}} \dot{q}_0 - \delta_{h,0} \quad (39)$$

In the asynchronous variant, the inversion augmentation is configured such that the angular acceleration and horizontal tail position feedback filter design elements can be designed independently. The synchronous variant represents a more constrained architecture in the sense that the matching strategy is enforced on the filter elements.

The control system properties corresponding to both design options after mixed μ -synthesis are presented in Fig. 5. A brief summary of the most relevant information can also be found in Table 1. The asynchronous and synchronous high-order control systems returned by the optimizer are obtained after 10 and 8 iterations and feature denominator orders of 66 and 62, respectively. Figures 5c and 5d show that both design variants yield solutions that satisfy the performance requirements in a robust sense, with peak $\bar{\mu}$ not exceeding the unity threshold value. Examining the diagrams more closely reveals that the optimized robust performance levels obtained for either implementation are in fact very close, which implies that the optimizer did not manage to extract more performance from the additional design degree of freedom in the asynchronous case. Consequently, imposing synchronous filter dynamics does not impose big limitations on the robust performance potential of the IDI-based control law, which confirms that the application of the matching strategy to filter design forms a reasonable design philosophy for managing the synchronization effect.

It is of additional interest to examine the SISO broken-loop response of the synchronous variant in Fig. 5b. Compared to the

basic design as shown in Fig. 4b, it is evident that the all-loops broken responses are nearly equivalent and that the loop shape with the actuator loop closed (point B in Fig. 1) reflects the principal tradeoffs associated with the design problem. In particular, the gain crossover frequency ω_c has moved to a lower region, while the low-to-medium frequency high gain characteristics that govern the robustness of the IDI control law against real perturbations have been largely maintained. Adequate phase margin in the crossover region has also been preserved.

B. The μ -Optimal Low-Order Synchronous Designs

The control laws returned by the full-order (unstructured) synthesis procedure are of very high order, which is a known characteristic of the *DGK*-iteration procedure. In this light, low-order, fixed-structure filter designs that can be implemented in practice need to be considered instead. The MATLAB Robust Control ToolboxTM [56] brings the possibility to optimize fixed-order controller structures based on nonsmooth H_∞ -synthesis [58], which is the procedure followed here. In view of the preceding discussion, the synchronous architecture will be adopted. The following fixed structures are selected, which correspond to second-order lag-lead and low-pass filters:

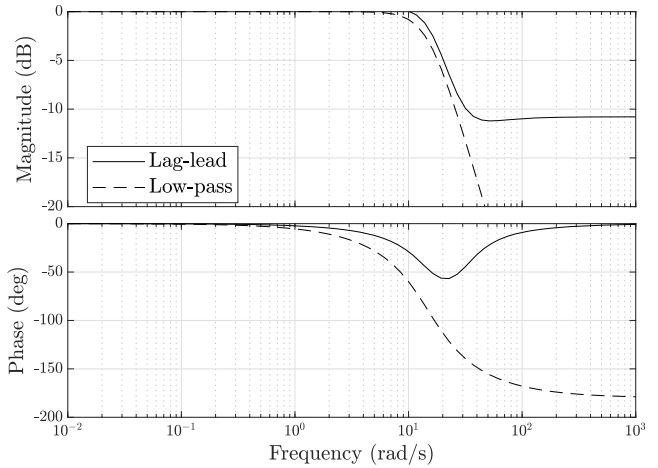
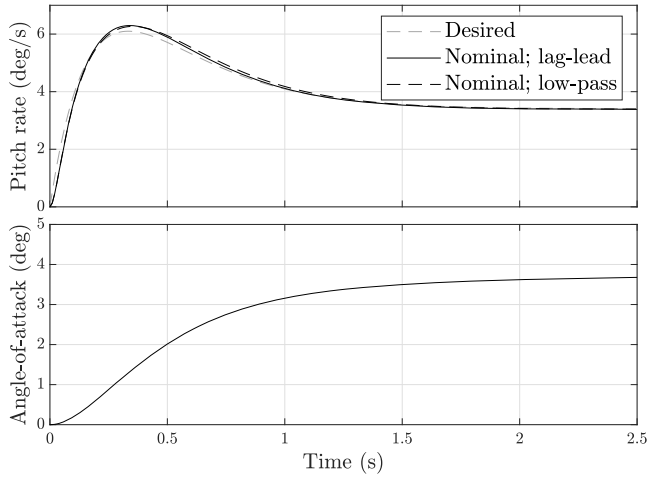
$$\begin{aligned} K(s) &= \frac{v_f(s)}{v_0(s)} = K_1(s) = \frac{u_f(s)}{u_0(s)} = K_2(s) = \frac{\dot{q}_f(s)}{\dot{q}_0(s)} \\ &= \frac{a_2 s^2 + a_1 s + a_0}{s^2 + b_1 s + b_0} \end{aligned} \quad (40)$$

$$K(s) = \frac{v_f(s)}{v_0(s)} = K_1(s) = \frac{u_f(s)}{u_0(s)} = K_2(s) = \frac{\dot{q}_f(s)}{\dot{q}_0(s)} = \frac{\omega_n^2}{s^2 + \sqrt{(1/2)}\omega_n s + \omega_n^2} \quad (41)$$

The reason for selecting these forms is that they are closely in line with previous successful designs [25,27,38]. The lag-lead architecture offers more flexibility compared to the low-pass design, for which only

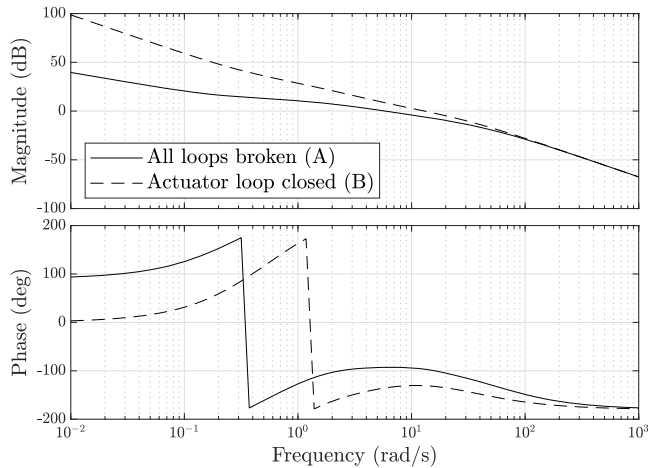
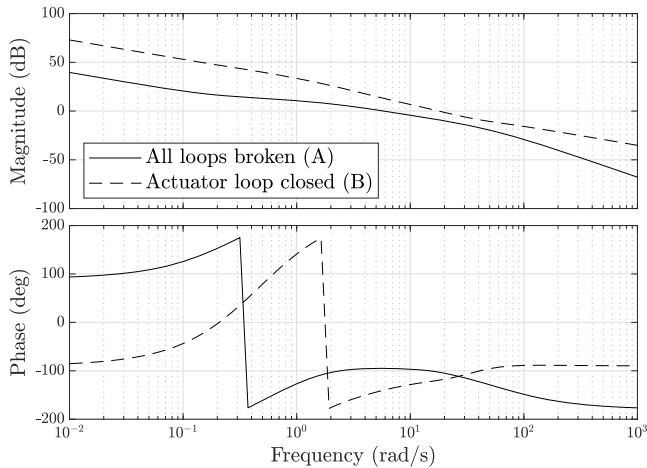
break frequency ω_n forms the available tuning parameter. The mixed μ -synthesis results are presented in Fig. 6 and Table 1.

With both designs, the performance requirements are met for the entire uncertainty set. However, the peak $\bar{\mu}$ of the low-pass architecture is higher compared to the lag-lead form, which shows very similar performance levels when compared to the full-order designs presented earlier. This forms a direct consequence of the additional design flexibility and is also reflected by the broken-loop response diagrams in Figs. 6c and 6d, which show that both the gain crossover frequency and phase margins are lower for the low-pass filter design



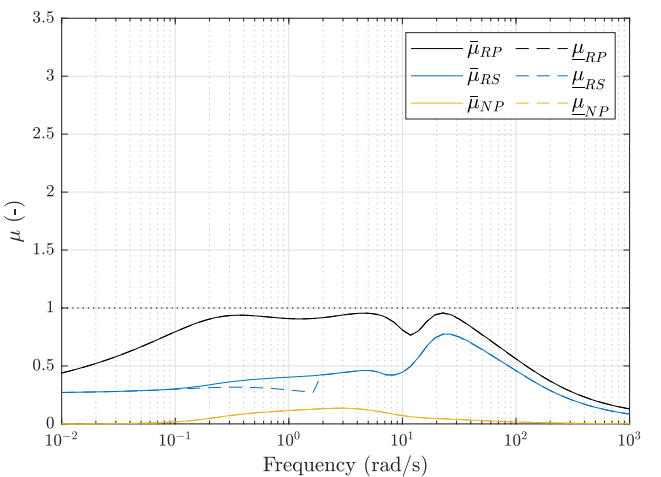
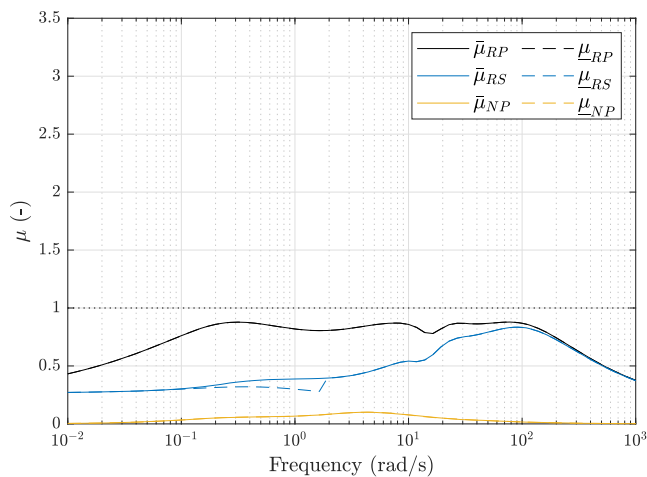
a) Step responses

b) Optimized filter designs



c) Broken-loop frequency response (lag-lead)

d) Broken-loop frequency response (low-pass)



e) Stability and performance margins (lag-lead)

f) Stability and performance margins (low-pass)

Fig. 6 Overview of low-order μ -optimal augmented IDI-based control system properties.

Table 1 Summary of control system peak robust performance levels and nominal broken-loop response characteristics [actuator feedback closed (B)]

Inversion design method	Sync. compensation	$\bar{\mu}_{RP}^*$	ω_c , rad/s	PM, deg
Dynamic inversion	n/a	2.10	5.98	83.5
Incremental dynamic inversion	Actuator sensor	1.59	60.3	84.0
	Actuator model	1.71	60.3	84.0
<i>IDI augmentation: full-order synthesized designs</i>				
Asynchronous	Actuator sensor	0.858	12.5	53.6
Synchronous	Actuator sensor	0.869	15.3	48.7
<i>IDI augmentation: low-order synthesized designs</i>				
Lag-lead, synchronous	Actuator sensor	0.879	17.4	59.6
	Actuator model	0.793	14.7	79.2
	Control command	0.789	14.6	81.1
Low-pass, synchronous	Actuator sensor	0.958	13.0	49.3
	Actuator model	0.973	11.0	50.8
	Control command	0.981	10.2	49.5

Note that ω_c is gain crossover frequency; PM, phase margin; n/a, not applicable.

option. Comparing both optimized filter designs in Fig. 6b leads to the conclusion that the smaller phase “reach back” associated with the lag-lead variant represents a key attribute. This demonstrates that mitigating phase distortions in the rigid-body frequency range should be considered as a design guideline, which is in line with the time-scale separation assumption that underlies the derivation of the control law. Still, these results also confirm that using synchronous low-pass filters should be viewed as a reasonable strategy when designing incremental dynamic-inversion-based control laws.

C. Reinstating Model Information

Although the matching strategy to filter design is shown to be successful in improving the overall robustness properties of IDI-based control laws, this comes at the cost of an enlarged inversion residual even in the nominal situation. This raises the question if and to what extent this disadvantage can be mitigated. Equation (15) suggests that the inversion residual can be further decreased by reintroducing model information of the bare airframe dynamics in the form of a complementary augmentation element. Based on the concept proposed in [59], this approach is used in [21] and is formulated in [60] as a hybrid INDI approach. It is of interest to investigate how this design method can improve upon the preceding sensor-based inversion strategies.

Additionally, there may be circumstances where direct actuator measurements may not be available. Although it can be expected that these are available in modern aircraft, this may not be the case for some unmanned aerial vehicles [25], for example. This implies that the control system architecture from Fig. 1 does not apply. In this case, another form of input signal feedback needs to be found. An internal model representation of the nominal actuator dynamics $H_a(s)$ would provide a solution here, which has been introduced in the past [25]. This strategy is illustrated in Fig. 7, together with a closely related design option that adopts direct control command feedback instead. Both variants will be compared in performance to the designs presented earlier.

1. Hybrid Incremental Dynamic Inversion

The basic principle of the hybrid inversion strategy is that any information that is distorted or lost as a result of the filter feedback augmentation system K is compensated for by adding complemen-

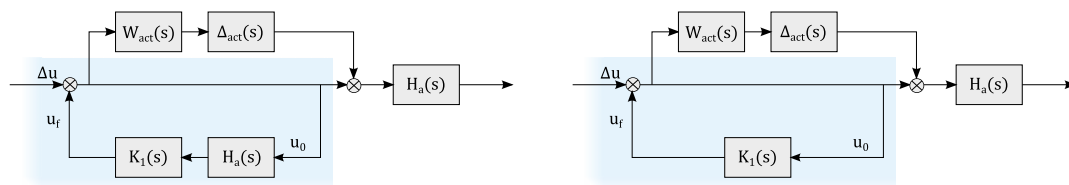
tary model information of the plant dynamics [60]. Using this design method, it can be shown that, in the nominal case where the control effectiveness is known and the only sources of singular perturbations are the augmentation filters themselves, the inversion residual expressed by Eq. (15) reduces to

$$\epsilon_{\text{INDI}}(\mathbf{x}, \Delta_2) = -\Delta_2 \xi(\mathbf{x}) \tag{42}$$

where $\Delta_2 = \Delta_1 = K - I$ in this case. It is noted that the resulting inversion residual depends solely on the onboard model error term $\xi(\mathbf{x})$. This shows that although high-quality models will lead to the smallest inversion residuals, low-fidelity complementary model information also positively contributes to the reduction of inversion error. The impact of other uncertainties is again considered by performing μ -analysis. For the F-16 design problem, the following design is used:

$$\hat{q}_{\text{fb}}(s) = K(s)\hat{q}(s) + (1 - K(s))\hat{q}(s) \triangleq K(s)\hat{q}(s) + K'(s)\hat{q}(s) \tag{43}$$

where $K(s)$ is selected as the low-pass filter design from Eq. (41) and $\hat{q}(s)$ follows from Eq. (37). Note that the same form is applied to the horizontal tail position feedback signal, which leads to an all-pass synchronization strategy. Figure 8 shows the results from a batch μ -analysis where the break frequency ω_n has been selected as the running variable. This diagram confirms that as the break frequency reduces, which corresponds to closer operating time-scales between the plant and filter feedback augmentation system, the hybrid approach results in enhanced levels of nominal and robust performance for similar stability margins. This is despite the fact that the onboard model error is significant for some plants in the uncertainty set. However, the general conclusion remains that, for maximum robust performance, filters shall be tuned sufficiently fast to meet the time-scale separation assumption. When high-frequency filters are used, adding model information does not yield significant tracking performance benefits other than an improved nominal response. Also, performance degradation can be expected for the hybrid approach in case of imperfect air data measurements, which is likely in practice [9].



a) Internal model feedback (AM)

b) Control command feedback (CC)

Fig. 7 Alternative synchronization compensation strategies.

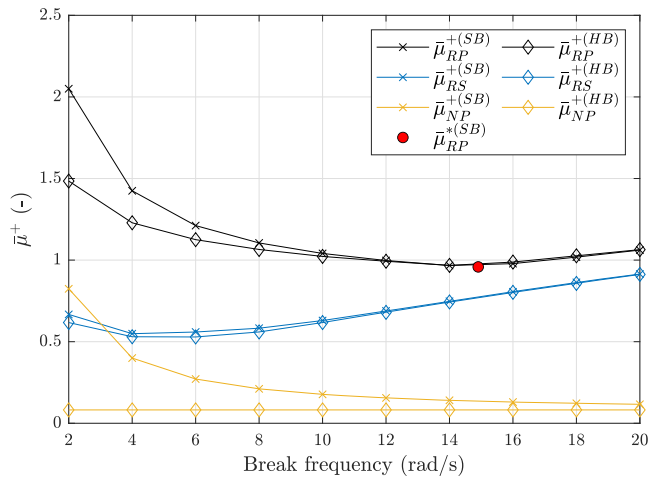


Fig. 8 Peak $\bar{\mu}$ trends as function of break frequency for low-pass-filtered sensor-based (SB) and hybrid (HB) IDI designs.

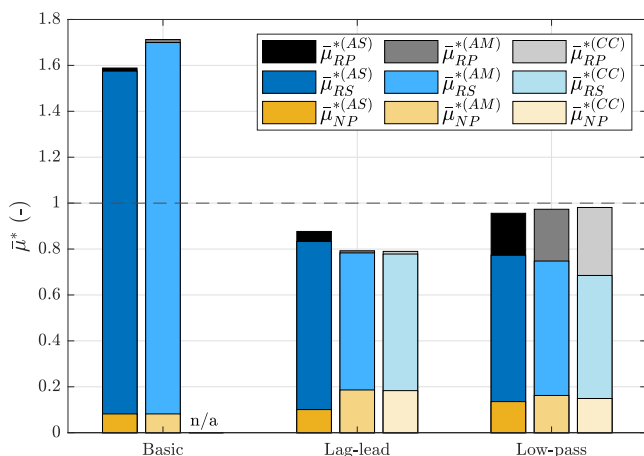


Fig. 9 Optimal $\bar{\mu}$ levels for basic and low-order synthesized IDI using actuator sensor (AS), actuator model (AM), or control command (CC) feedback.

2. Alternative Synchronization Compensation

Figure 9 illustrates the relative peak performance levels found for the alternative synchronization strategies from Fig. 7. Both basic (no filter augmentation) and optimized low-order designs are considered. Comparing these to the results presented earlier, it can be seen that both strategies deliver satisfactory robust performance levels if adequate filtering is in place. Therefore, viable designs may be found even in case no actuator sensor instrumentation is available. In case of sufficient bandwidth separation between the nominal actuator dynamics and augmentation filters, even the use of an internal model may not be required.

D. Overview

An overview of the numerical results presented in the preceding sections is shown in Table 1. The matching strategy has been found to be an adequate strategy for handling the synchronization effect in the presence of dynamic uncertainty. Robustness against aerodynamic variations is largely maintained and is not heavily affected by adopting low-order designs. This also holds in case internal actuator models are used, if adequate feedback filters are in place.

V. Conclusions

The stability and performance robustness characteristics of INDI against regular and possibly unknown singular perturbations have been investigated in this paper. For traditional NDI, the inversion residual that arises under these perturbations may grow large in magnitude, but can always be described at a given state by an

upper bound under modest assumptions. By contrast, INDI shows improved robustness to regular perturbations, but its inversion residual may grow unbounded under similar conditions for particular combinations of singular perturbations. This corresponds to a loss of robust stability as a result of the synchronization effect. By introducing additional augmentation to sensor feedback signals, the robustness properties of INDI can be further improved.

A linear control law design study based on the structured singular value (μ) framework confirms that IDI features increased levels of robustness to aerodynamic uncertainties, at the expense of robust stability due to unknown singular perturbations. The matching strategy, which has been applied successfully in the past, is shown to be a reasonable design method to compensate for the synchronization effect and compares closely in terms of optimized robustness levels to less-constrained asynchronous design options. The use of additional model information as a form of complementary augmentation can further improve the design in case the time-scale separation assumption is violated due to low-bandwidth feedback filter designs. In case actuator sensor measurements are not available, alternative synchronization strategies can still lead to adequately performing designs.

Finally, the applicability and limitations of the presented robustness insights should be emphasized. First, only input-affine systems and singular perturbations that can be described by linear mappings have been considered in this work. Second, closed-loop effects of nonlinear or time-varying dynamics have not been addressed. Therefore, the results lead to an elementary understanding of the robustness properties of INDI-based control laws only. This implies that, in order to handle the full complexity of nonlinear control laws and bare airframe dynamics as well as other uncertainty classes, more powerful analysis strategies must be considered.

References

- [1] Anon., "Flight Control Design—Best Practices," NATO Research and Technology Organization (RTO) RTO-TR-029, 2000.
- [2] Anon., *Flying Qualities of Piloted Aircraft*, U.S. Department of Defense, MIL-HDBK-1797A, 1997.
- [3] Anon., *Airworthiness Certification Criteria*, U.S. Department of Defense, MIL-HDBK-516C, 2014.
- [4] Tauke, G., and Bordignon, K., "Structural Coupling Challenges for the X-35B," *2002 Biennial International Powered Lift Conference and Exhibit*, AIAA Paper 2002-6004, 2002. <https://doi.org/10.2514/6.2002-6004>
- [5] Moorhouse, D. J., "Lessons Learned in the Development of a Multivariable Control System (STOL and S/MTD Programs)," *Proceedings of the IEEE National Aerospace and Electronics Conference*, IEEE Publ., Piscataway, NJ, 1989, pp. 364–371. <https://doi.org/10.1109/NAECON.1989.40236>
- [6] Blight, J. D., Dailey, R. L., and Gangsaas, D., "Practical Control Law Design for Aircraft Using Multivariable Techniques," *International Journal of Control*, Vol. 59, No. 1, 1994, pp. 93–137. <https://doi.org/10.1080/00207179408923071>
- [7] "Application of Multivariable Control Theory to Aircraft Control Laws, Final Report: Multivariable Control Design Guidelines," Honeywell Technology Center, Lockheed Martin Skunk Works and Lockheed Martin Tactical Aircraft Systems WL-TR-96-3099, 1996.
- [8] Balas, G. J., "Flight Control Law Design: An Industry Perspective," *European Journal of Control*, Vol. 9, No. 2, 2003, pp. 207–226. <https://doi.org/10.3166/ejc.9.207-226>
- [9] Enns, D., Bugajski, D., Hendrick, R., and Stein, G., "Dynamic Inversion: An Evolving Methodology for Flight Control Design," *International Journal of Control*, Vol. 59, No. 1, 1994, pp. 71–91. <https://doi.org/10.1080/00207179408923070>
- [10] Harris, J. J., and Stanford, J. R., "F-35 Flight Control Law Design, Development and Verification," *2018 Aviation Technology, Integration, and Operations Conference*, AIAA Paper 2018-3516, 2018. <https://doi.org/10.2514/6.2018-3516>
- [11] Canin, D., McConnell, J. K., and James, P. W., "F-35 High Angle of Attack Flight Control Development and Flight Test Results," *AIAA Aviation 2019 Forum*, AIAA Paper 2019-3227, 2019. <https://doi.org/10.2514/6.2019-3227>
- [12] Wang, X., van Kampen, E., Chu, Q. P., and Lu, P., "Stability Analysis for Incremental Nonlinear Dynamic Inversion Control," *Journal of*

- Guidance, Control, and Dynamics*, Vol. 42, No. 5, 2019, pp. 1116–1129. <https://doi.org/10.2514/1.G003791>
- [13] Smith, P., “A Simplified Approach to Nonlinear Dynamic Inversion Based Flight Control,” *23rd Atmospheric Flight Mechanics Conference*, AIAA Paper 1998-4461, 1998. <https://doi.org/10.2514/6.1998-4461>
- [14] Smith, P., and Berry, A., “Flight Test Experience of a Non-Linear Dynamic Inversion Control Law on the VAAC Harrier,” *Atmospheric Flight Mechanics Conference*, AIAA Paper 2000-3914, 2000. <https://doi.org/10.2514/6.2000-3914>
- [15] Sieberling, S., Chu, Q. P., and Mulder, J. A., “Robust Flight Control Using Incremental Nonlinear Dynamic Inversion and Angular Acceleration Prediction,” *Journal of Guidance, Control, and Dynamics*, Vol. 33, No. 6, 2010, pp. 1732–1742. <https://doi.org/10.2514/1.49978>
- [16] Simplício, P., Pavel, M. D., van Kampen, E., and Chu, Q. P., “An Acceleration Measurements-Based Approach for Helicopter Nonlinear Flight Control Using Incremental Nonlinear Dynamic Inversion,” *Control Engineering Practice*, Vol. 21, No. 8, 2013, pp. 1065–1077. <https://doi.org/10.1016/j.conengprac.2013.03.009>
- [17] Azinheira, J., Moutinho, A., and Carvalho, J., “Lateral Control of Airship with Uncertain Dynamics Using Incremental Nonlinear Dynamics Inversion,” *IFAC-PapersOnLine*, Vol. 48, No. 19, 2015, pp. 69–74. <https://doi.org/10.1016/j.ifacol.2015.12.012>
- [18] Francesco, G. D., and Mattei, M., “Modeling and Incremental Nonlinear Dynamic Inversion Control of a Novel Unmanned Tiltrotor,” *Journal of Aircraft*, Vol. 53, No. 1, 2016, pp. 73–86. <https://doi.org/10.2514/1.C033183>
- [19] Beyer, Y., Kuzolap, A., Steen, M., Diekmann, J. H., and Fezans, N., “Adaptive Nonlinear Flight Control of STOL-Aircraft Based on Incremental Nonlinear Dynamic Inversion,” *2018 Modeling and Simulation Technologies Conference*, AIAA Paper 2018-3257, 2018. <https://doi.org/10.2514/6.2018-3257>
- [20] Lombaerts, T., Kaneshige, J., Schuet, S., Aponso, B. L., Shish, K. H., and Hardy, G., “Dynamic Inversion Based Full Envelope Flight Control for an eVTOL Vehicle Using a Unified Framework,” *AIAA SciTech 2020 Forum*, AIAA Paper 2020-1619, 2020. <https://doi.org/10.2514/6.2020-1619>
- [21] Yang, Y., Wang, X., Zhu, J., Yuan, X., and Zhang, X., “Robust Proportional Incremental Nonlinear Dynamic Inversion Control of a Flying-Wing Tailsitter,” *Proceedings of the Institution of Mechanical Engineers, Part G: Journal of Aerospace Engineering*, Vol. 234, No. 16, 2020, pp. 2274–2295. <https://doi.org/10.1177/0954410020926657>
- [22] Chen, G., Liu, A., Hu, J., Feng, J., and Ma, Z., “Attitude and Altitude Control of Unmanned Aerial-Underwater Vehicle Based on Incremental Nonlinear Dynamic Inversion,” *IEEE Access*, Vol. 8, Aug. 2020, pp. 156,129–156,138. <https://doi.org/10.1109/ACCESS.2020.3015857>
- [23] Fuest, H., Duda, D. F., Islam, T., and Moormann, D., “Flight Control Architecture of a Flying Wing for Vertical Take-Off and Landing of an Airborne Wind Energy System,” *AIAA SciTech 2021 Forum*, AIAA Paper 2021-1816, 2021. <https://doi.org/10.2514/6.2021-1816>
- [24] Luo, F., Zhang, J., Lyu, P., Liu, Z., and Tang, W., “Carrier-Based Aircraft Precision Landing Using Direct Lift Control Based on Incremental Nonlinear Dynamic Inversion,” *IEEE Access*, Vol. 10, May 2022, pp. 55709–55725. <https://doi.org/10.1109/ACCESS.2022.3175164>
- [25] Smeur, E. J. J., Chu, Q. P., and de Croon, G. C. H. E., “Adaptive Incremental Nonlinear Dynamic Inversion for Attitude Control of Micro Air Vehicles,” *Journal of Guidance, Control, and Dynamics*, Vol. 39, No. 3, 2016, pp. 450–461. <https://doi.org/10.2514/1.G001490>
- [26] van Ekeren, W., Looye, G., Kuchar, R. O., Chu, Q. P., and Van Kampen, E., “Design, Implementation and Flight-Tests of Incremental Nonlinear Flight Control Methods,” *2018 AIAA Guidance, Navigation, and Control Conference*, AIAA Paper 2018-0384, 2018. <https://doi.org/10.2514/6.2018-0384>
- [27] Grondman, F., Looye, G., Kuchar, R. O., Chu, Q. P., and Van Kampen, E., “Design and Flight Testing of Incremental Nonlinear Dynamic Inversion-Based Control Laws for a Passenger Aircraft,” *2018 AIAA Guidance, Navigation, and Control Conference*, AIAA Paper 2018-0385, 2018. <https://doi.org/10.2514/6.2018-0385>
- [28] Raab, S. A., Zhang, J., Bhardwaj, P., and Holzapfel, F., “Proposal of a Unified Control Strategy for Vertical Take-Off and Landing Transition Aircraft Configurations,” *2018 Applied Aerodynamics Conference*, AIAA Paper 2018-3478, 2018. <https://doi.org/10.2514/6.2018-3478>
- [29] Keijzer, T., Looye, G., Chu, Q. P., and Van Kampen, E., “Design and Flight Testing of Incremental Backstepping Based Control Laws with Angular Accelerometer Feedback,” *AIAA SciTech 2019 Forum*, AIAA Paper 2019-0129, 2019. <https://doi.org/10.2514/6.2019-0129>
- [30] Pollack, T., Looye, G., and van der Linden, F., “Design and Flight Testing of Flight Control Laws Integrating Incremental Nonlinear Dynamic Inversion and Servo Current Control,” *AIAA SciTech 2019 Forum*, AIAA Paper 2019-0130, 2019. <https://doi.org/10.2514/6.2019-0130>
- [31] Binz, F., Islam, T., and Moormann, D., “Attitude Control of Tiltwing Aircraft Using a Wing-Fixed Coordinate System and Incremental Nonlinear Dynamic Inversion,” *International Journal of Micro Air Vehicles*, Vol. 11, July 2019, Paper 1756829319861370. <https://doi.org/10.1177/1756829319861370>
- [32] Smeur, E. J. J., Bronz, M., and de Croon, G. C. H. E., “Incremental Control and Guidance of Hybrid Aircraft Applied to a Tailsitter Unmanned Air Vehicle,” *Journal of Guidance, Control, and Dynamics*, Vol. 43, No. 2, 2020, pp. 274–287. <https://doi.org/10.2514/1.G004520>
- [33] Pfeifle, O., and Fichter, W., “Cascaded Incremental Nonlinear Dynamic Inversion for Three-Dimensional Spline-Tracking with Wind Compensation,” *Journal of Guidance, Control, and Dynamics*, Vol. 44, No. 8, 2021, pp. 1559–1571. <https://doi.org/10.2514/1.G005785>
- [34] Tal, E., and Karaman, S., “Accurate Tracking of Aggressive Quadrotor Trajectories Using Incremental Nonlinear Dynamic Inversion and Differential Flatness,” *IEEE Transactions on Control Systems Technology*, Vol. 29, No. 3, 2021, pp. 1203–1218. <https://doi.org/10.1109/TCST.2020.3001117>
- [35] Tal, E. A., and Karaman, S., “Global Trajectory-Tracking Control for a Tailsitter Flying Wing in Agile Uncoordinated Flight,” *AIAA Aviation 2021 Forum*, AIAA Paper 2021-3214, 2021. <https://doi.org/10.2514/6.2021-3214>
- [36] Steinleitner, A., Frenzel, V., Pfeifle, O., Denzel, J., and Fichter, W., “Automatic Take-Off and Landing of Tailwheel Aircraft with Incremental Nonlinear Dynamic Inversion,” *AIAA SciTech 2022 Forum*, AIAA Paper 2022-1228, 2022. <https://doi.org/10.2514/6.2022-1228>
- [37] Khalil, H., *Nonlinear Systems*, 3rd ed., Pearson Education, Prentice-Hall, Upper Saddle River, NJ, 2002, Chaps. 5, 11 and 13.
- [38] van’t Veld, R., van Kampen, E., and Chu, Q. P., “Stability and Robustness Analysis and Improvements for Incremental Nonlinear Dynamic Inversion Control,” *2018 AIAA Guidance, Navigation, and Control Conference*, AIAA Paper 2018-1127, 2018. <https://doi.org/10.2514/6.2018-1127>
- [39] Pavel, M. D., Shanthakumaran, P., Chu, Q. P., Stroosma, O., Wolfe, M., and Cazemier, H., “Incremental Nonlinear Dynamic Inversion for the Apache AH-64 Helicopter Control,” *Journal of the American Helicopter Society*, Vol. 65, No. 2, 2020, pp. 1–16. <https://doi.org/10.4050/JAHS.65.022006>
- [40] Huang, Y., Zhang, Y., Pool, D. M., Stroosma, O., and Chu, Q. P., “Time-Delay Margin and Robustness of Incremental Nonlinear Dynamic Inversion Control,” *Journal of Guidance, Control, and Dynamics*, Vol. 45, No. 2, 2022, pp. 394–404. <https://doi.org/10.2514/1.G006024>
- [41] Cordeiro, R. A., Marton, A. S., Azinheira, J. R., Carvalho, J. R. H., and Moutinho, A., “Increased Robustness to Delay in Incremental Controllers Using Input Scaling Gain,” *IEEE Transactions on Aerospace and Electronic Systems*, Vol. 58, No. 2, 2022, pp. 1199–1210. <https://doi.org/10.1109/TAES.2021.3123215>
- [42] Chang, J., Breuker, R. D., and Wang, X., “Discrete-Time Design and Stability Analysis for Nonlinear Incremental Fault-Tolerant Flight Control,” *AIAA SciTech 2022 Forum*, AIAA Paper 2022-2034, 2022. <https://doi.org/10.2514/6.2022-2034>
- [43] Skogestad, S., and Postlethwaite, I., *Multivariable Feedback Control: Analysis and Design*, 2nd ed., Wiley, New York, 2005, Chaps. 7 and 8.
- [44] Stein, G., “Respect the Unstable,” *IEEE Control Systems Magazine*, Vol. 23, No. 4, 2003, pp. 12–25. <https://doi.org/10.1109/MCS.2003.1213600>
- [45] Stevens, B., Lewis, F., and Johnson, E., *Aircraft Control and Simulation: Dynamics, Controls Design, and Autonomous Systems*, Wiley, Hoboken, NJ, 2015, Chaps. 2 and 6.
- [46] Gong, A., Tischler, M. B., and Hess, R. A., “Deterministic Reconfiguration of Flight Control Systems for Multirotor UAV Package Delivery,” *Vertical Flight Society’s 77th Annual Forum & Technology*

- Display*, Vertical Flight Soc., Fairfax, VA, 2021.
<https://doi.org/10.4050/F-0077-2021-16865>
- [47] Kim, C.-S., Ji, C.-H., Koh, G.-O., and Kim, B. S., "Stability Margin and Structural Coupling Analysis of a Hybrid INDI Control for the Fighter Aircraft," *International Journal of Aeronautical and Space Sciences*, Vol. 22, No. 5, 2021, pp. 1154–1169.
<https://doi.org/10.1007/s42405-021-00394-8>
- [48] Balas, G., Garrard, W., and Reinder, J., "Robust Dynamic Inversion Control Laws for Aircraft Control," *Guidance, Navigation and Control Conference*, AIAA Paper 1992-4329, 1992.
<https://doi.org/10.2514/6.1992-4329>
- [49] Adams, R., and Banda, S., "Robust Flight Control Design Using Dynamic Inversion and Structured Singular Value Synthesis," *IEEE Transactions on Control Systems Technology*, Vol. 1, No. 2, 1993, pp. 80–92.
<https://doi.org/10.1109/87.238401>
- [50] Reigelsperger, W. C., and Banda, S. S., "Nonlinear Simulation of a Modified F-16 with Full-Envelope Control Laws," *Control Engineering Practice*, Vol. 6, No. 3, 1998, pp. 309–320.
[https://doi.org/10.1016/S0967-0661\(98\)00024-0](https://doi.org/10.1016/S0967-0661(98)00024-0)
- [51] Valasek, J., Ito, D., and Ward, D., "Robust Dynamic Inversion Controller Design and Analysis for the X-38," *AIAA Guidance, Navigation, and Control Conference and Exhibit*, AIAA Paper 2001-4380, 2001.
<https://doi.org/10.2514/6.2001-4380>
- [52] Kolesnikov, E., "NDI-Based Flight Control Law Design," *AIAA Guidance, Navigation, and Control Conference and Exhibit*, AIAA Paper 2005-5977, 2005.
<https://doi.org/10.2514/6.2005-5977>
- [53] Bacon, B., and Ostroff, A., "Reconfigurable Flight Control Using Non-linear Dynamic Inversion with a Special Accelerometer Implementation," *AIAA Guidance, Navigation, and Control Conference and Exhibit*, AIAA Paper 2000-4565, 2000.
<https://doi.org/10.2514/6.2000-4565>
- [54] Isidori, A., *Nonlinear Control Systems*, 3rd ed., Springer Science & Business Media, London, 1995, Chap. 4.
- [55] Wang, X., van Kampen, E., Chu, Q. P., and Lu, P., "Incremental Sliding-Mode Fault-Tolerant Flight Control," *Journal of Guidance, Control, and Dynamics*, Vol. 42, No. 2, 2019, pp. 244–259.
<https://doi.org/10.2514/1.G003497>
- [56] Balas, G., Chiang, R., Packard, A., and Safonov, M., *Robust Control Toolbox™ Reference*, MathWorks, Inc., Natick, MA, 2022.
- [57] Russell, R., "Non-Linear F-16 Simulation Using Simulink and Matlab," Univ. of Minnesota TR Ver. 1.0, Minneapolis, MN, 2003.
- [58] Apkarian, P., and Noll, D., "Nonsmooth H_∞ Synthesis," *IEEE Transactions on Automatic Control*, Vol. 51, No. 1, 2006, pp. 71–86.
<https://doi.org/10.1109/TAC.2005.860290>
- [59] Jiali, Y., and Jihong, Z., "An Angular Acceleration Estimation Method Based on the Complementary Filter Theory," *2016 IEEE International Instrumentation and Measurement Technology Conference Proceedings*, IEEE Publ., Piscataway, NJ, 2016.
<https://doi.org/10.1109/I2MTC.2016.7520548>
- [60] Kumtepe, Y., Pollack, T., and van Kampen, E., "Flight Control Law Design Using Hybrid Incremental Nonlinear Dynamic Inversion," *AIAA SciTech 2022 Forum*, AIAA Paper 2022-1597, 2022.
<https://doi.org/10.2514/6.2022-1597>